Phase Transition in Hydrogen-Bonded 1-Adamantane-methanol

Bacem Ben Hassine, Philippe Negrier, Maria Barrio, Denise Mondieig, Stéphane Massip, Josep Lluis Tamarit

Phase Transition in Hydrogen-Bonded 1-Adamantane-methanol

Bacem Ben Hassine,[†,§] Philippe Negrier,[†] María Barrio,[‡] Denise Mondieig,[†] Stéphane Massip,[∥] and Josep Ll. Tamarit*[,‡]

[†]LOMA, UMR 5798, F 33400 Talence, France, CNRS, LOMA, UMR 5798, Université de Bordeaux, F 33400 Talence, France

[‡]Grup de Caracterització de Materials, Department de Física i Enginyeria Nuclear, ETSEIB, Diagonal 647, Universitat Politècnica de Catalunya, 08028 Barcelona, Catalonia, Spain

[§]Laboratoire des Matériaux Céramiques Composites et Polymères, LaMaCoP, Département Physique, Faculté des Sciences de Sfax, 3000 Sfax, Tunisia

[∥]Institut Européen Chimie & Biologie, Université de Bordeaux, CNRS UMS 3033, INSERM US001, F 33607 Pessac, France

ABSTRACT: The polymorphism of 1 adamantane methanol $C_{11}H_{18}O$ has been investigated by differential thermal analysis and single crystal and powder X ray diffraction. Below the melting temperature (389.5 ± 0.4 K), this compound exhibits an orthorhombic phase (phase I, *Pnnm*, $Z = 12$, $Z' = 1.5$). The melting enthalpy was determined to be 20.5 ± 0.4 kJ mol^{-1}, i.e., with an entropy change of (6.34 ± 0.13)R, which is much higher than the quoted value from Timmermans for the melting orientationally disordered phases (2.5R), thus supporting the orientationally ordered character of phase I. This orthorhombic phase I exhibits a statistical disorder of the hydrogen atom related to the oxygen atom, due to the position of one independent molecule on the mirror. At ca. 272 K, phase I transforms continuously through an order−disorder transition to a low temperature monoclinic phase II ($P2_1/n$, $Z = 12$, $Z' = 3$). The monoclinic and orthorhombic phases are related by a group−subgroup relationship, which perfectly agrees with the continuous character of the II to I transition. Moreover, by a convenient choice of an order parameter related to the continuous tilt of the *c* axis, the critical exponent for this transition is found to be close to the theoretical prediction of the three dimensional Ising model (with a critical exponent of ca. 0.27).

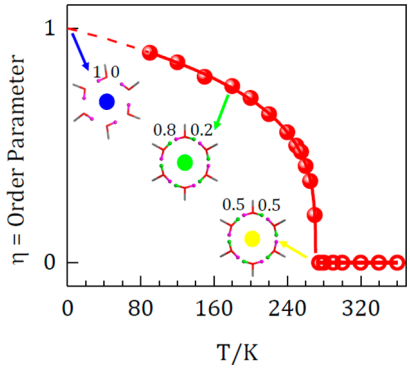

1. INTRODUCTION

Diamondoids are organic compounds with unique structures and properties. This family of compounds is one of the best candidates for a self assembled process in a large number of applications as chemical processes, many applications in nanotechnology as well as in biological and pharmaceutical domains.[1−6]

Diamondoids have recently acquired great interest owing to their important role in industrial chemicals, in particular, for building up organic crystals with large cavities and useful physical and chemical properties.[7−12]

The simplest member of the diamondoid group is the adamantane molecule, $C_{10}H_{16}$, which is a rigid molecule with point group symmetry T_d formed by 10 carbon atoms arranged as a single diamond cage surrounded by 16 hydrogen atoms.[13]

Recently, adamantane derivative molecules have been used for gel systems by mixing 1 adamantanecarboxylic acid and 1 adamantylamine owing to the hydrogen bonding between carboxylic acid and amine groups.[14] This system is seen as a colloidal system with nanometer particles (formed by the aforementioned molecules strongly linked) interacting through van der Waals forces.

The replacement of one or more hydrogen atoms in the molecule of adamantane by a substituent X (X = OH, F, Cl, I, etc.) modifies the symmetry of the molecule, its polarity, intermolecular interactions, and steric effects, in particular, in solid phases. There are two positions on the adamantane cage where single substitution can occur: the 1 X position, with a highly reactive tertiary carbon, where the molecule retains a C_{3v} point group symmetry, and the 2 X position, with a secondary less reactive carbon atom, which gives rise to molecules with C_{2v} symmetry. Although the number of studies concerning 2 X adamantane derivatives is less extensive, detailed polymorphic studies have also been reported.[15−22]

The phase behavior of the 1 X adamantane compounds varies according to the substituent. Most of these derivatives show up an orientationally disordered (plastic) phase prior to fusion, for example, 1 chloroadamantane, 1 bromoadamantane, and 1 cyanoadamantane. However, in the case of 1 iodoadamantane, the high temperature phase is not orienta tionally disordered.[23−26]

These compounds also may have one or several solid−solid transitions. For example, 1 chloroadamantane and 1 bromoa damantane exhibit one and two solid−solid phase transitions,

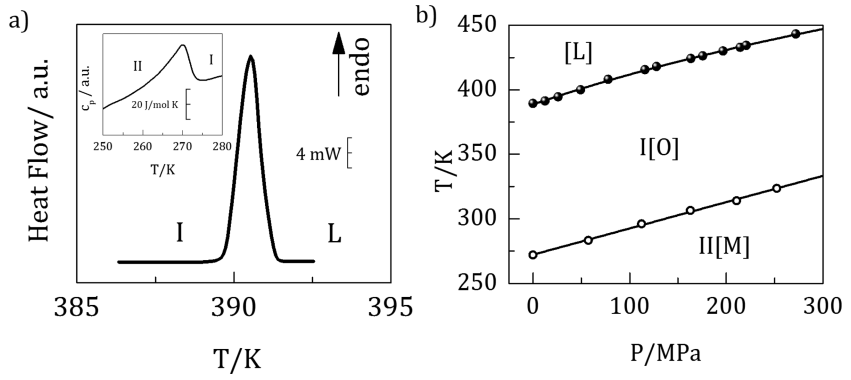

Figure 1. (a) DTA curve of the solid to liquid transition for 1 adamantane methanol. Inset: Relative specific heat across the solid−solid transition.(b) Solid−solid (empty circles) and melting (full circles) transition temperature curves as a function of pressure.

respectively.[27] These adamantane derivatives show a rich polymorphic behavior that has largely been studied.[28−36]

The physical and chemical properties, even for the simple adamantane derivatives, have not been studied for some of them in which the substitution concerns more than a halogen atom. Among these adamantane derivatives, 1 CH_2OH adamantane (1 adamantane methanol, $C_{11}H_{18}O$) is one for which no studies have been conducted until the present. In this paper, the polymorphism of this compound and the mechanisms of solid−solid transitions have been undertaken by means of a combination of several experimental techniques, thermal analysis and powder and single crystal X ray diffraction. The structures for the different phases have been determined and compared for the first time.

2. EXPERIMENTAL DETAILS

2.1. Materials. 1 Adamantane methanol ($C_{11}H_{18}O$) was purchased from Sigma Aldrich with a purity of 99%. It was used after further purification by sublimation under partial vacuum at 323 K.

2.2. Differential Thermal Analysis. The thermal properties of the phase transitions (temperature and enthalpy changes) were determined by a PerkinElmer DSC 7 instrument. Heating and cooling rates of (2 K·min^{-1} and 10 K·min^{-1}) under a constant nitrogen stream and powder samples with mass between 4 mg and 10 mg were used. A TA Instruments Q100 system was used with an intracooler system for the low temperature specific heat measurements through the modulation function. In such a case, scanning rates of 1 K·min^{-1} with modulation of ±0.5 K every 60 s were used.

2.3. High-Pressure Differential Thermal Analysis. The transitions were studied with homemade high pressure differential thermal analyzers (HP DTA) for low and for high temperature.[37] These systems enabled us to cover a temperature range between 200 and 470 K within a pressure range from normal pressure to 300 MPa. Samples were sealed in cylindrical tin pans by melting the studied substance taking care that no residual air remains. HP DTA scans were carried out with a heating rate of 2 K·min^{-1}.

2.4. Powder X-ray Diffraction Measurements. Powder X ray diffraction data were collected by means of a horizontally mounted INEL cylindrical position sensitive detector (CPS 120). The detector, used in Debye−Scherrer geometry, is constituted by channels, providing an angular step of 0.029° (2θ) between 4° and 120°. Monochromatic Cu $K_{\alpha 1}$ radiation (λ = 1.5406 Å) was selected with an asymmetric focusing incident beam curved quartz monochromator. The angular linearity deviation in position sensitive detector (PSD) was corrected according to the recommended procedure with external calibration and was performed by means of cubic spline fittings.[38] We used the $Na_2Ca_2Al_2F_{14}$ cubic phase mixed with silver behenate. The generator power was set to 1.0 kW (40 kV and 25 mA). The peak positions were determined by pseudo Voigt fittings using the Peakoc application from Diffractinel software.[39] The samples were introduced into 0.5 mm diameter Lindemann capillaries which rotate along their longitudinal axes during data collection to prevent the effects of the preferred orientations. The system is equipped with a liquid nitrogen 600 series Cryostream Cooler from Oxford Cryosystems with a temperature accuracy of 0.1 K and similar to fluctuations. The X ray profiles were acquired isothermally after cooling and heating back so that the temperature range was scanned at the intervals of 20 K and less when the transition was approached.

The indexing of the X ray powder diffraction patterns, structure solutions, Pawley and Rietveld refinements were performed using Materials Studio Program (MS Modeling (Materials Studio), version 5.5; http://www.accelrys.com).[40]

2.5. Single-Crystal X-ray Diffraction Measurements. Several single crystals with different morphologies were picked from the raw product. Because of the twining tendency, a very small single crystal (0.20 × 0.12 × 0.08 mm^3) was chosen.

The single crystal X ray diffraction data were collected at 275 K with an FR X Rigaku diffractometer with rotating anode Cu−K_α radiation (λ = 1.54187 Å) and a Dectris Pilatus 200 K detector. The unit cell determination and data reduction were performed using the Crystal Clear program suite[41] on the full set of data. The structure was solved by direct methods and refined using Shelx 97[42] suite of programs in the integrated WinGX system.[43] The positions of the H atoms were deduced from the coordinates of the non H atoms and confirmed by Fourier synthesis. The non H atoms were refined with anisotropic temperature parameters.

3. RESULTS AND DISCUSSION

The normal pressure thermal analysis of 1 adamantane methanol was performed from 250 K up to the melting. The thermograms (Figure 1a) have revealed a spread out endothermal effect peaking at ca. 272 K associated with a solid−solid transition and an endothermic peak corresponding to the melting, T_{onset} = 389.5 ± 0.4 K, with an enthalpy change of 20.5 ± 0.4 kJ mol^{-1}. The inset of Figure 1 depicts the specific heat C_p measured by means of modulated calorimetry across the II to I transition. The shape of C_p variation with temperature is clearly reminiscent of a high order phase transition. Both II to I and I to liquid temperature transitions increased on increasing pressure (Figure 1b). The II−I curve is found to be linear ($T = ap + T_0$ with a = 0.203 ± 0.004 MPa^{-1} and T_0 = 272.27 ± 0.69 K), whereas the melting curve is slightly convex, i.e., dT/dp decreases on increasing pressure. In that case, the Anderson Anderson equation $T = k_1(1 + (k_2/k_3)p)^{1/k_2}$[44] was used for describing the experimental points. The best fit (solid line in Figure 1b) was obtained for k_1 = 388.6 ± 0.4 K, k_2 =4.9 ± 0.6, and k_3 = 1487 ± 68. Within the limit of p

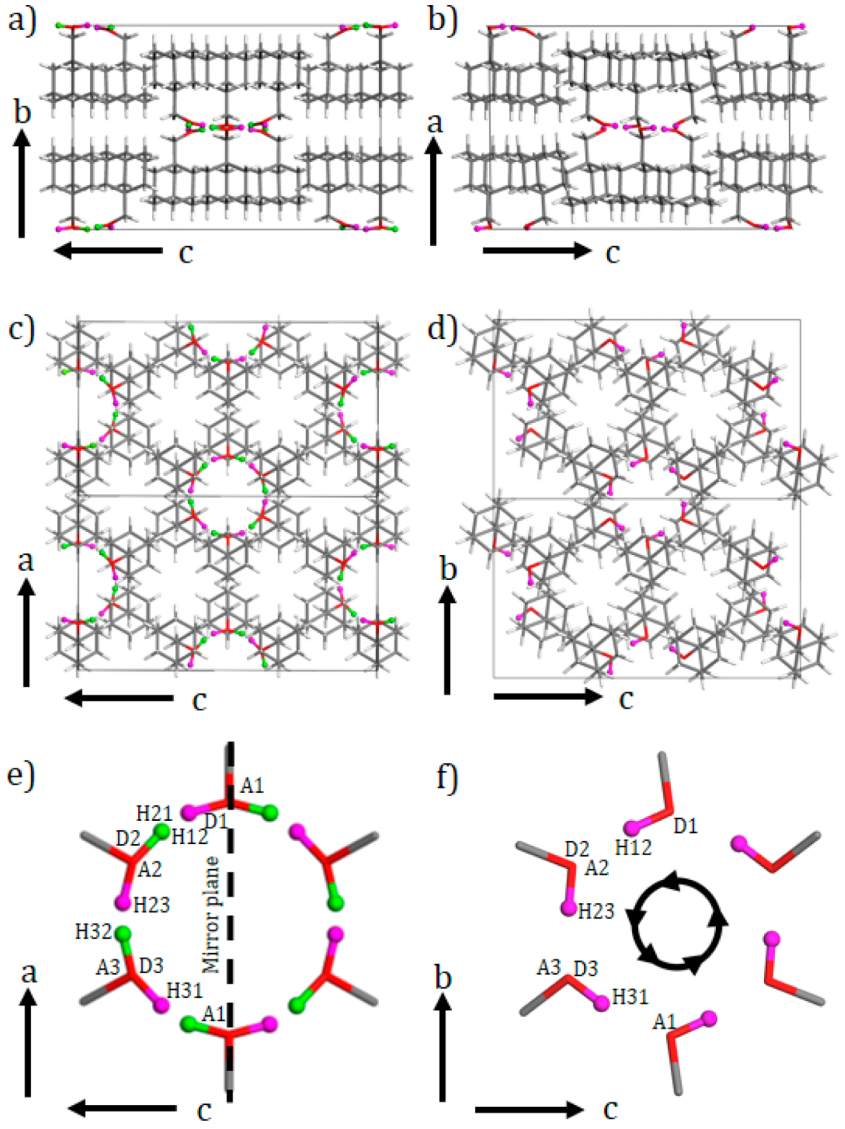

Figure 2. Crystal structures of 1 adamantane methanol phase I at 275 K (left panels, (a) along *a* and (c) along *b*) and phase II at 90 K (right panels, (b) along *b* and (d) along *a*). Panels (e) and (f) depict the intermolecular hydrogen bond scheme for phases I (along *b* planes) and II (along *a* planes), respectively. A and D indicate the acceptor and donor character of the oxygen atoms.

$\rightarrow 0$, $((dT/dp))_{p\rightarrow 0} = (k_1/k_3) = (0.261 \pm 0.012)$ K·MPa^{-1}. According to the Clausius−Clapeyron equation, $((dT/dp)) = (\Delta v/\Delta s) = (T\Delta v/\Delta h)$, where Δs and Δh are the entropy and the enthalpy changes at the transition, a volume change at the melting temperature T of $(\Delta v = v_L - v_s = 13.8 \pm 0.6)$ cm^3·mol^{-1} is inferred. Such a volume change provides a relative volume change of $(v_L/v_s) = 1.29 \pm 0.05$, with $v_s = 152.7$ cm^3·mol^{-1}, is the volume of the solid phase obtained at the melting point by extrapolating the values obtained by means of X ray diffraction, which agrees with the values obtained for many organic systems, for which $(v_L/v_s) = 1.10 \pm 0.07$.[45] In addition, it must be mentioned that both the volume change at the melting and the slope of the two phase coexistence curve, $((dT/dp))$, are close to the volume change at the ordered to orientationally disordered transition for some adamantane derivatives,[46−48] thus reinforcing the orientationally ordered character of phase I for the case here studied. Moreover, the changes of the thermodynamic properties at the melting process do not correlate with the relationships established for orientationally disordered phases.[49,50]

The structure of phase I was solved by means of high resolution X ray single crystal diffraction patterns at 275 K. The lattice of phase I was determined as orthorhombic, space group *Pnnm* and $Z = 12$. There are two independent molecules, one molecule in a general position and the other one on the mirror, so $Z' = 1.5$ (see Figure 2a,c). This orthorhombic phase exhibits a statistical disorder concerning the hydrogen atom related to the oxygen atom, due to the position of the independent molecule on the mirror. In order to highlight this disorder, the hydrogen atoms whose occupancy rate is 0.5 are represented by full green and pink circles.

The cohesion of the structure is ensured both by hydrogen bonds and van der Waals interactions alternatively (see Figure 2a,b). Figure 2e shows the arrangement of the hydrogen bonds in phase I at 275 K. The structure consists of a three dimensional (3D) hydrogen bond network along the *b* plane but connecting molecules along the *b* axis (see Figure 2a) in such a way that six molecules form a hexagon shaped structure (Figure 2e) in which molecular dipoles point to. The intermolecular distances O···O of hydrogen bond are between

2.628 and 2.644 Å, and the angles O−H···O range from 154° to 158° for the two independent molecules (see Table 1). These

Table 1. Hydrogen Bond Angles (O−H···O) and Distances (O···O) for Phases I and II

phase	angles O H O	(deg)	distances O O	(Å)
I	D1 H12 A2	154	D1 A2	2.628
	D2 H21 A1	157	D2 A1	2.628
	D3 H32 A2	158	D3 A2	2.644
II	D1 H12 A2	172	D1 A2	2.587
	D2 H23 A3	171	D2 A3	2.604
	D3 H31 A1	168	D3 A1	2.725

results reflect strong hydrogen bonds and consistently strong intermolecular interactions. The existence of a mirror implies that the hydrogen bond related to oxygen is disordered, and then the hydrogen atoms attached to the oxygen atom have an occupancy factor of 0.5. Such strong interactions consist of the high value of the melting entropy change, (6.34 ± 0.13)R, i.e., much higher than the characteristic value of 2.5R established by Timmermans[51] as an upper bound for orientationally disordered (plastic) phases. On these grounds, 1 adamantane methanol is one of the few 1 X adamantane derivatives without a high temperature orientationally disordered phase.

On cooling from phase I to phase II, the single crystal was always damaged, so the structure of phase II was undertaken through high resolution X ray powder diffraction. The lattice of the low temperature phase II was determined at 90 K as monoclinic by means of X Cell software, available in the module Powder Indexing of Materials Studio. Systematic absences enable us to determine the space group, which was compatible with the $P2_1/n$ space group, and according to a reasonable density and compatibility between the zero volume change at the II−I transition, $Z = 12$ was assigned. Pawley refinement,[52] which minimizes the weighted R factor, R_{wp}, describing the agreement between the experimental and the simulated patterns, helps to confirm the indexing result and the systematic absences, thus confirming the space group. The unit cell parameters refined are gathered in Table 2. The final Rietveld refinement,[53] position, and orientation of the molecule, within the rigid body constraint, with a single overall isotropic displacement parameter and preferred orientation were refined using the Rietveld−Toraya function.[54] The final refined pattern is depicted in Figure 3 together with the experimental and refined pattern difference. The representation of the structure obtained for phase II is displayed in Figure 2d (in this figure the hydrogen atoms are represented by full pink circles). Broadly speaking, the overall packing of phase II is quite similar to that of phase I, with the obvious difference of the breakdown of the mirror plane. The arrangement of the hydrogen bonds for phase II at 90 K is presented in Figure 2f. The shorter O···O hydrogen bonds distances in phase II are 2.587 and 2.604 Å, with O−H···O angles of 172° and 171°, close but shorter than those present in phase I, indicating a slightly stronger intermolecular interactions.

In order to check the intermolecular interactions, the isobaric thermal expansion tensor has been determined.[55−57]

To do so, lattice parameters as a function of temperature from 90 to 360 K were measured (see Table S1). Patterns were collected every 30 K and every 5 K close to the II−I transition. The variation of the lattice parameters with temperature is shown in Figure 4a,d. For the continuity in the settings, we

Table 2. Crystal Data for Phases I and II of 1 Adamantane methanol from the X ray Single Crystal and Powder Diffraction Analyses, Respectively

structure	phase II	phase I
formula	$C_{11}H_{18}O$	$C_{11}H_{18}O$
FW (g mol^{-1})	166.25	166.25
crystal system	monoclinic	orthorhombic
space group	$P2_1/n$	$Pnnm$
T (K)	90(2)	275(2)
wavelength (Å)	1.5406	1.54187
unit cell dimensions (Å)	a = 13.0675(7)	a = 11.4489(8)
	b = 11.2831(8)	b = 13.1094(9)
	c = 19.3721(14)	c = 19.6876(14)
	α = 90°	α = 90°
	β = 90.518°(5)	β = 90°
	γ = 90°	γ = 90°
Z (Z')	12(3)	12(1.5)
V (Å^3)	2856.1(3)	2954.9(4)
D_x (g cm^{-3})	1.160	1.121
R_{wp}	4.69%	
R_p	3.32%	
R_1, ($I > 2\sigma(I)$)		6.9%
wR_2, ($I > 2\sigma(I)$)		16.75%
R_1		10.65%
wR_2		18.15%

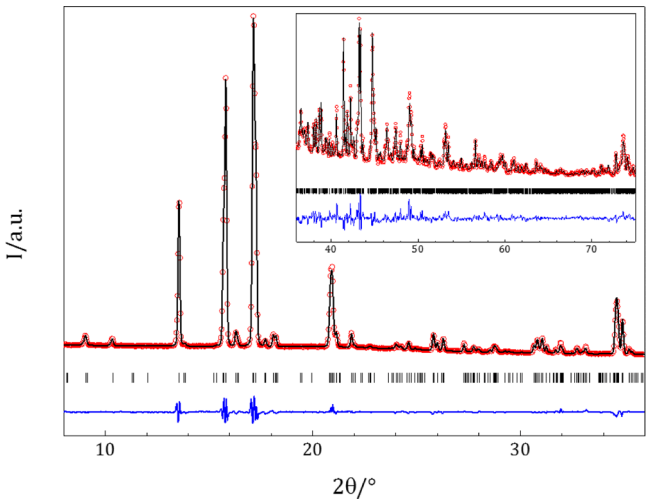

Figure 3. Experimental (red circles) and Rietveld refined (black line) diffraction patterns along with the difference profile (blue line) and Bragg reflections (vertical sticks) of the monoclinic $P2_1/n$ space group phase II of 1 adamantane methanol at 90 K. Inset corresponds to the scale for the data between 35° and 75° magnified 10 times.

present a_{II} with b_I and b_{II} with a_I. The continuity in the variation of the parameters and the volume (see Figure 4) as a function of temperature indicate that the phase change is provided by a second order transition with virtually no volume change, as revealed by the thermodynamic measurements.

The lattice parameters and unit cell volume were fitted by a standard least squares method as a function of temperature, and the polynomials describing such a temperature variation are compiled in Table S2.

The thermal expansion tensors are represented in Figure 5 for three temperatures. For the monoclinic phase, the tensor is defined by the principal coefficients, α_1, α_2, and α_3 and an angle between the principal direction and the crystallographic 2 fold

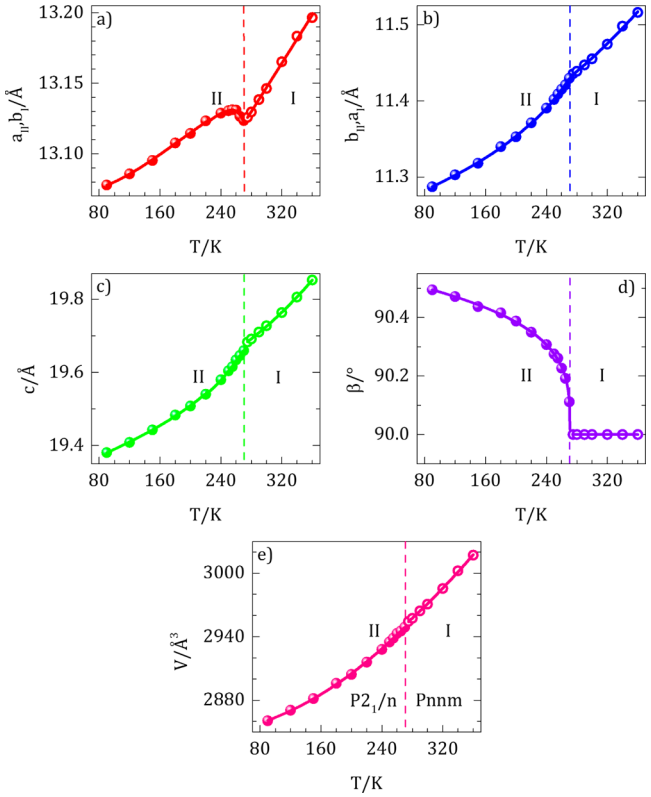

Figure 4. Variation of the lattice parameters and the volume as a function of temperature for phases II (full circles) and phase I (empty circles). Lines are the polynomial fits (see Table S2 in Supporting Information). The error bars are smaller than the size of the points.

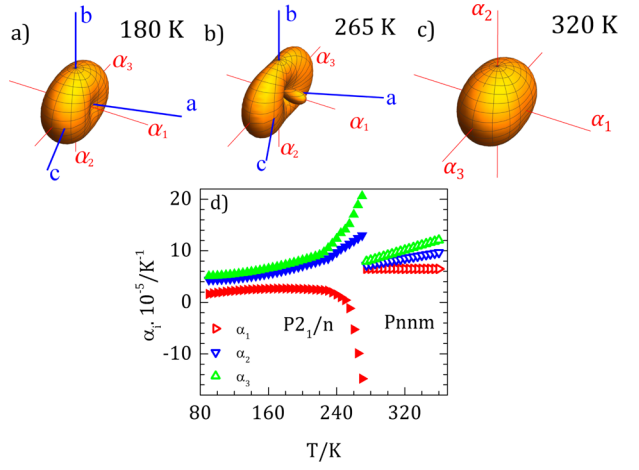

Figure 5. Thermal expansion tensors for $P2_1/n$ monoclinic phase II (a and b) and *Pnnm* orthorhombic phase I (c) and the eigenvalues α_i for the orthorhombic (empty symbols) and monoclinic (full symbols) phases as a function of temperature (d).

axis *b*, while for the orthorhombic phase, the eigenvectors are coincident with the crystal axes. Figure 5d shows the variations of the eigenvalues as a function of temperature for the two phases. Although the hydrogen bonds are mainly in the (*bc*) plane, the thermal expansion reveals stronger interactions in the direction α_1 (the "hard" direction) close to *a*, in which even negative values (contraction) are found. The soft direction, i.e., that with the weakest interaction (α_3) lies within the (00l) plane. Such a direction for phase II becomes softer when approaching the II to I transition, due to the oncoming appearance of the mirror plane.

According to the temperature variation of the β parameter (see Figure 4d) in which the β angle changes continuously on cooling from 90° around T_c to higher values and the subgroup−group relation between phase I and phase II, an order parameter η for a continuous (second order) II to I transition can be defined as

$$\eta(T) = \eta_0 + (\beta(T=0) - 90°)\left[1 - \frac{T}{T_c}\right]^{\gamma} \quad (1)$$

where $\eta_0 = 90°$ is the orthorhombic angle of phase I, $\beta(T-0)$ is the β angle at $T = 0$ K, T_c is the critical transition temperature, and γ is the critical exponent. A fit of eq 1 to the phase II data gives rise to $T_c = 270.71 \pm 0.18$ K, close to the calorimetric phase transition, and $\gamma = 0.269 \pm 0.004$, close to the theoretical prediction of 3D microscopic Ising model, i.e., 0.33.[58]

This order−disorder phase transition can be interpreted microscopically by means of the disorder of the H atom linked to the O atom, lying on the mirror, in phase II, as it is for phase I, in which the H atom displays an occupancy factor of 50% (in both sides of the mirror plane, Figure 2e). Thus, on cooling phase II the H atom would increase the difference of the occupational factor between the two sites, as described in Figure 2f. In fact, at 90 K, the lowest temperature at which the structure has been solved, the occupancy factor of 1 of the sites (pink atom) is close to 1, with values of the angles of the hydrogen bonds close to 180° (the arrows in Figure 2f indicate the direction of the most probable direction of donor, acceptor directions). Within this image the decrease of the order parameter on increasing temperature (Figure 6) would be

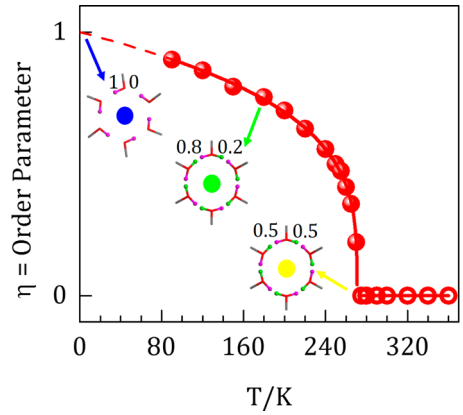

Figure 6. Order parameter η as a function of temperature for monoclinic phase I (full circles) and orthorhombic phase II (empty circles). Line corresponds to the fit according to eq 1. Pictures along the order parameter curve are hydrogen bond schemes with the occupational factor for the hydrogen of the −OH group.

accompanied by an increase of the "symmetrization" of the occupational factor of the H atom of the hydroxyl group up to equal values (50%) at $T = T_c$, the temperature at which the equality of the occupational factors (together with the value of $\beta = 90°$) makes the appearance of the symmetry plane and thus leading to the lattice the *Pnnm* symmetry. Second order phase transitions involving organic hydrogen bonded crystals have recently been described,[59−61] and even a Landau theory using an expansion of the free energy has been proposed.[62,63]

4. CONCLUSION

The polymorphism of 1 adamantane methanol has been studied from 90 K to the liquid state. The low temperature phase II, which was found to be monoclinic with space group $P2_1/n$ (Z = 12, Z' = 3) transforms to the high temperature phase I with space group $Pnnm$ (Z = 12, Z' = 1.5). The passage from the monoclinic phase to the orthorhombic phase is conducted by means of a second order phase transition which carries a group−subgroup relationship, and its order is proved by a continuous tilt of the c axis. The resolution of the crystal structures of both phases was carried out by exploiting X ray diffraction data on powder (phase II) and on single crystal (phase I). Both structures have a very close stacking of molecules with strong hydrogen bonds. Although both phases are built up through a 12 molecules per unit lattice, the number of independent molecules is reduced through a second order phase transition which breaks the mirror symmetry present in phase I. The pressure−temperature phase diagram does not reveal the appearance of new phases. The volume and entropy change at the melting as well as the slope $((dT/dp))_{I\rightarrow L}$ of the two phase coexistence curve thermodynamically reinforce the disordered character of phase I highlighted by the structural study, unlike most of 1 X adamantane derivatives.

AUTHOR INFORMATION

Corresponding Author

*E mail: josep.lluis.tamarit@upc.edu.

Notes

The authors declare no competing financial interest.

ACKNOWLEDGMENTS

This work has been partially supported by the Spanish Ministry of Science and Innovation through Project FIS2014 54734 P and by the Generalitat de Catalunya under Project 2014 SGR 581.

REFERENCES

(1) Wang, Y. Y.; Kiopakis, E.; Lu, X. H.; Wegner, D.; Yamachika, R.; Dahl, J. E.; Carlson, R. M. K.; Louie, S. G.; Crommie, M. F. *Nat. Mater.* **2008**, *7*, 38−42.

(2) Yang, W. L.; Fabbri, J. D.; Willey, T. M.; Lee, J. R. I.; Dahl, J. E.; Carlson, R. M. K.; Schreiner, P. R.; Fokin, A. A.; Tkachenko, B. A.; Fokina, N. A.; Meevasana, W.; Mannella, N.; Tanaka, K.; Zhou, X. J.; van Buuren, T.; Kelly, M. A.; Hussain, Z.; Melosh, N. A.; Shen, Z. X. *Science* **2007**, *316*, 1460−1462.

(3) Du, Q. S.; Huang, R. B. *Curr. Protein Peptide Sci.* **2012**, *13*, 205−210.

(4) De Clercq, E. *J. Clin. Virol.* **2004**, *30*, 115−133.

(5) Nicholson, K. G.; Wood, J. M.; Zambon, M. *Lancet* **2003**, *362*, 1733−1745.

(6) Cheon, Y. E.; Suh, M. P. *Chem. Eur. J.* **2008**, *14*, 3961−3967.

(7) Elsaidi, S. K.; Mohamed, M. H.; Wojtas, L.; Chanthapally, A.; Pham, T.; Space, B.; Vittal, J. J.; Zaworotko, M. J. *J. Am. Chem. Soc.* **2014**, *136*, 5072−5077.

(8) Schoedel, A.; Zaworotko, M. *J. Chem. Sci.* **2014**, *5*, 1269−1282.

(9) Yamamoto, A.; Uehara, S.; Hamada, T.; et al. *Cryst. Growth Des.* **2012**, *12*, 4600−4606.

(10) Gunawan, M. A.; Hierso, J. C.; Poinsot, D.; et al. *New J. Chem.* **2014**, *38*, 28−41.

(11) Hohman, J. N.; Claridge, Sh. A; Kim, M.; Weiss, P. S. *Mater. Sci. Eng., R* **2010**, *70*, 188−208.

(12) McIntosh, G. C.; Yoon, M.; Berber, S.; Tomanek, D. *Phys. Rev. B: Condens. Matter Mater. Phys.* **2004**, *70*, 045401.

(13) Vijayakumar, V.; Garg, A. B.; Godwal, B. K.; Sikka, S. K. *Chem. Phys. Lett.* **2000**, *330*, 275−280.

(14) Zhang, M.; Zukoski, Ch. F. *Langmuir* **2014**, *30*, 7540−7546.

(15) Negrier, Ph.; Barrio, M.; Tamarit, J. Ll.; Mondieig, D. *J. Phys. Chem. B* **2014**, *118*, 9595−9603.

(16) Bazyleva, A. B.; Blokhin, A. V.; Kabo, G. J.; Kabo, A. G.; Sevruk, V. M. *Thermochim. Acta* **2006**, *451*, 65−72.

(17) Romanini, M.; Negrier, P.; Tamarit, J. Ll.; Capaccioli, S.; Barrio, M.; Pardo, L. C.; Mondieig, D. *Phys. Rev. B: Condens. Matter Mater. Phys.* **2012**, *85*, 134201.

(18) Harvey, P. D.; Butler, I. S.; Gilson, D. F. R.; Wong, P. T. T. *J. Phys. Chem.* **1986**, *90*, 4546−4549.

(19) Negrier, P.; Barrio, M.; Romanini, M.; Tamarit, J. Ll.; Mondieig, D.; Krivchikov, A. I.; Kepinski, L.; Jezowski, A.; Szewczyk, D. *Cryst. Growth Des.* **2014**, *14*, 2626−2632.

(20) Hara, K.; Katou, Y.; Osugi, J. *Bull. Chem. Soc. Jpn.* **1981**, *54*, 687−691.

(21) Paroli, R. M.; Kawaii, A. T.; Butler, A. S.; Gilson, D. R. *Can. J. Chem.* **1988**, *66*, 1973−1978.

(22) Hara, K.; Taniguchi, J.; Suzuki, K. *Chem. Lett.* **1980**, *7*, 803−806.

(23) Clark, T.; Mckervey, M. A.; Mackle, H.; Rooney, J. J. *J. Chem. Soc., Faraday Trans. 1* **1974**, *70*, 1279−1291.

(24) Foulon, M.; Grors, C. *Acta Crystallogr., Sect. B: Struct. Sci.* **1988**, *44*, 156−163.

(25) Foulon, M.; Amoureux, J. P.; Sauvajol, J. L.; Lefebvre, J.; Descamps, M. *J. Phys. C: Solid State Phys.* **1983**, *16*, L265−L269.

(26) Martinez Garcia, J. C.; Tamarit, J. Ll.; Capaccioli, S.; Barrio, M.; Veglio, N.; Pardo, L. C. *J. Chem. Phys.* **2010**, *132*, 164516.

(27) Clark, T.; Knox, T. M. O.; Mackle, H.; Mckervey, M. A. *J. Chem. Soc., Faraday Trans. 1* **1977**, *73*, 1224−1231.

(28) Virlet, J.; Quiroga, L.; Boucher, B.; Amoureux, J. P.; Castelain, M. *Mol. Phys.* **1983**, *48*, 1289−1303.

(29) Braga, D.; Koetzle, T. F. *Acta Crystallgr. B* **1988**, *44*, 156−163.

(30) Decressain, R.; Amoureux, J. P.; Carpentier, L.; Nagy, J. B. *Mol. Phys.* **1991**, *73*, 553−569.

(31) Foulon, M.; Belgrand, T.; Gors, C.; More, M. *Acta Crystallogr., Sect. B: Struct. Sci.* **1989**, *45*, 404−411.

(32) Affouard, F.; Hedoux, A.; Guinet, Y.; Denicourt, T.; Descamps, M. *J. Phys.: Condens. Matter* **2001**, *13*, 7237−7248.

(33) Amoureux, J. P.; Sauvajol, J. L.; Bee, M. *Acta Crystallogr., Sect. A: Cryst. Phys., Diffr., Theor. Gen. Crystallogr.* **1981**, *37*, 97−104.

(34) Amoureux, J. P.; Bee, M.; Sauvajol, J. L. *Acta Crystallogr., Sect. B: Struct. Crystallogr. Cryst. Chem.* **1982**, *38*, 1984−1989.

(35) Bee, M.; Amoureux, J. P. *Mol. Phys.* **1983**, *48*, 63−79.

(36) Betz, R.; Klüfers, P.; Mayer, P. *Acta Crystallogr., Sect. E: Struct. Rep. Online* **2009**, *65*, o101.

(37) Manosa, Ll.; Gonzalez Alonso, D.; Planes, A.; Bonnot, E.; Barrio, M.; Tamarit, J. Ll.; Aksoy, S.; Acet, M. *Nat. Mater.* **2010**, *9*, 478−481.

(38) Ballon, J.; Comparat, V.; Pouxe, J. *Nucl. Instrum. Methods Phys. Res.* **1983**, *217*, 213−216.

(39) Evain, M.; Deniard, P.; Jouanneaux, A.; Brec, R. *J. Appl. Crystallogr.* **1993**, *26*, 563−569.

(40) *MS Modeling* (Materials Studio), version 5.5: http://www.accelrys.com.

(41) *Crystalclear sm expert 2.1 Software*, Rigaku, 2013.

(42) Sheldrick, G. M. *Acta Crystallogr., Sect. A: Found. Crystallogr.* **2008**, *64*, 112−122.

(43) Farrugia, L. J. *J. Appl. Crystallogr.* **1999**, *32*, 837−838.

(44) Andersson, S. P.; Anderson, O. *Macromolecules* **1998**, *31*, 2999−3006.

(45) Barrio, M.; Maccaroni, E.; Rietlveld, I. B.; Malpezzi, L.; Masciocchi, N.; Céolin, R.; Tamarit, J. Ll. *J. Pharm. Sci.* **2012**, *101*, 1073−1078.

(46) Negrier, P.; Barrio, M.; Tamarit, J. Ll.; Mondieig, D. *J. Phys. Chem. B* **2014**, *118*, 9595−9603.
(47) Negrier, P.; Barrio, M.; Romanini, M.; Tamarit, J. Ll.; Mondieig, D.; Krivchikov, A. I.; Kepinski, L.; Jezowski, A.; Szewczyk, D. *Cryst. Growth Des.* **2014**, *14*, 2626−2632.
(48) Hara, K.; Katou, Y.; Osugi, J. *Bull. Chem. Soc. Jpn.* **1981**, *54*, 687−691.
(49) Tamarit, J. Ll.; Rietveld, I. B.; Barrio, M.; Ceolin, R. *J. Mol. Struct.* **2014**, *1078*, 3−9.
(50) Reuter, J.; Busing, D.; Tamarit, J. Ll.; Wurflinger, A. *J. Mater. Chem.* **1997**, *7*, 41−46.
(51) Timmermans, J. *J. Phys. Chem. Solids* **1961**, *18*, 1−8.
(52) Pawley, G. S. *J. Appl. Crystallogr.* **1981**, *14*, 357−361.
(53) Rietveld, H. M. *J. Appl. Crystallogr.* **1969**, *2*, 65−71.
(54) Toraya, H.; Marumo, F. *Mineral. J.* **1981**, *10*, 211−221.
(55) Salud, J.; Barrio, M.; Lopez, D. O.; Tamarit, J. Ll.; Alcobé, X. *J. Appl. Crystallogr.* **1998**, *31*, 748−757.
(56) Tamarit, J. Ll.; Lopez, D. O.; Alcobé, X.; Barrio, M.; Salud, J.; Pardo, L. C. *Chem. Mater.* **2000**, *12*, 555−563.
(57) Negrier, P.; Pardo, L. C.; Salud, J.; Tamarit, J. Ll.; Barrio, M.; Lopez, D. O.; Würflinger, A.; Mondieig, D. *Chem. Mater.* **2002**, *14*, 1921−1929.
(58) Pelissetto, A.; Vicari, E. *Phys. Rep.* **2002**, *368*, 549−727.
(59) Chantrapromma, S.; Fun, H. K.; Usman, A. *J. Mol. Struct.* **2006**, *789*, 30−36.
(60) Ye, H. Y.; Ge, J. Z.; Chen, F.; Xiong, R. G. *CrystEngComm* **2010**, *12*, 1705−1708.
(61) How, P. T.; Lee, B. S.; Fun, H. K.; Razak, I. A.; Chantrapromma, S. *Phys. Rev. B* **2005**, *71*, 174109.
(62) Fun, H. K.; Usman, A.; Chantrapromma, S.; Osman, J.; Ong, L. H.; Tilley, D. R.; Ishibashi, Y. *Solid State Commun.* **2003**, *127*, 677−682.
(63) Rosli, M. M.; Lee, B. S.; Fun, H. K. *Phys. Status Solidi B* **2009**, *246*, 376−382.